JOURNAL OF CATALYSIS 123, 195–205 (1990)

# Electron Paramagnetic Resonance Spectroscopy Studies of Eu–Y and Coexchanged EuFe–Y Zeolites

M. A. ULLA,[1,*] L. A. APARICIO,[†] V. R. BALSE,[†] J. A. DUMESIC,[†] AND W. S. MILLMAN[2,*]

*Laboratory of Surface Studies, Department of Chemistry, University of Wisconsin, Milwaukee, Wisconsin 53201; and †Department of Chemical Engineering, University of Wisconsin, Madison, Wisconsin 53706

Received August 14, 1989; revised October 30, 1989

Electron paramagnetic resonance (EPR) was used to probe the oxidation state of europium and the location of divalent europium cations in Eu–Y and EuFe–Y zeolite samples. Europium was present as trivalent cations following treatment in $O_2$ at 770 K. Treatments in $H_2$ or CO at 770 K led to formation of divalent cations, and perhaps also caused some reduction to lower oxidation states. Three EPR signals were observed for $Eu^{2+}$, giving rise to effective $g$ values of 3, 4.9, and 6. The first and last signals are interpreted as being due to $Eu^{2+}$ cations at sites I and II, respectively, while the latter signal is due to $Eu^{2+}$ cations at sites I′ and II′. The majority of the $Eu^{2+}$ cations are at site I, and the amount of Eu at this site can be increased by reducing the sample in $H_2$, compared with reduction in CO. The presence of europium in site I forces the $Fe^{2+}$ cations to occupy sites of lower coordination in the sodalite unit (sites I′ and II′) and in the supercages (sites II and III′). 

## INTRODUCTION

Previous studies (*1–4*) have shown that the redox catalytic activity of base-exchanged zeolites depends on the nature of the exchange cation, the nature of the zeolite framework, and the location of the cations within that framework. The effect of varying the framework is illustrated by a comparison of Fe–Y and Fe–M. While both have about the same specific activity, the latter is significantly more active per iron cation (*2*). The effect of changing the location of the cations within the matrix is illustrated using Fe–Y zeolite and varying the silicon-to-aluminum ratio. Besides decreasing the base-exchange capacity, the activity per iron cation increased, as did the specific activity. As the silicon-to-aluminum ratio increased, the fraction of Fe cations occupying site I decreased while the fraction in sites I′, II′, and/or II, or possibly III′ increased (*4*).

The cation location in Y zeolite may also be modified by coexchange with a second cation, as shown recently (*1*). When the cations are Eu and Fe, Mössbauer spectroscopy showed that Eu alters the location of the Fe cations in the same manner as increasing the silicon-to-aluminum ratio. However, Fe also has an effect on Eu. For example, Eu–Y shows little catalytic activity for the reaction of CO with $O_2$ and it is difficult to reduce (*1*); however, when both Fe and Eu are present, the zeolite is both more active and more easily reduced.

Unfortunately it has not been possible to interpret fully the catalytic properties of mixed-cation catalysts, because the effect that Fe has on the location of Eu cations has not been determined. Thus, we have undertaken an investigation of the cation siting of Eu–Y and Eu–Fe–Y zeolites using EPR spectroscopy, which has been shown to be sensitive to the location of the $Eu^{2+}$ cations (*9*). These results are reported, along with Mössbauer spectroscopy studies of the $Fe^{2+}$ cations which were not reported earlier (*1*).

[1] On leave from INCAPE, Santa Fe, Argentina.
[2] To whom all correspondence should be addressed.



0021-9517/90 $3.00

## EXPERIMENTAL

The samples of Eu–Y and EuFe–Y were the same as those used in our earlier work (*1, 11*). The preparation was described previously (*1*), and the unit cell composition and cation loadings are the following: Eu–Y: $Si_{142}Al_{50}Na_{12}Eu_{13}O_{384}$; $5.70 \times 10^{20}$ Eu cations/g; EuFe–Y: $Si_{140}Al_{52}Na_9Eu_8Fe_{10}O_{384}$; $3.58 \times 10^{20}$ Eu and $4.47 \times 10^{20}$ Fe cations/g. The compositions are based on duplicate chemical analysis from Galbraith Laboratories where the agreement between the duplicates is better than 2% of the quantity of the individual elements. The unit cell compositions are based on the sum of the framework cations (Si and Al) totaling 192.

Thermal stability and redox chemistry were studied gravimetrically using a Cahn electrobalance (Model C-2000) in a flow mode. The experimental conditions were the same as those previously described (*3*).

Temperatures reported here are ±1 K with the exception of room temperature which is 296 ± 3 K.

EPR spectra were obtained using a Varian E-115 spectrometer at X-band frequency (9.2 GHz). Spectra were recorded at sample temperatures of 296 and 77 K. Sample treatments were carried out in a quartz reactor having a 4-mm-o.d. quartz EPR side-arm into which the sample could be transferred. All $g$ values reported were referenced to Varian strong pitch which has an isotropic $g$ value centered at 2.0028. Treatments such as reduction and oxidation or CO oxidation reactions using different $CO/O_2$ ratios were carried out in a flow system (100 ml/min). The samples were pretreated by heating at 5 K/min to progressively higher temperatures of 373, 473, 573, 673, and 773 K. The samples were kept under He flow until a temperature of 573 K had been reached, and then $O_2$ (25%) diluted in He was added. The samples were held at each of the preceding temperatures for 40 min and maintained at 773 K for 40–100 h. This oxidation pretreatment was carried out before every reduction. Reductions were carried out under either $H_2$ (25%) or CO (25%) diluted in He carrier gas. After each pretreatment, oxidation, reduction, or reaction, the sample was purged with flowing He for 5 min at 773 K and then cooled to room temperature and evacuated to $10^{-3}$ Torr.

The spectra of reduced Eu–Y at X-band frequency were simulated using the program POW (*5*). Spin concentrations were determined by the method described elsewhere (*6*). The spin standard used was a Varian strong pitch sample which had been previously calibrated against a NBS single-crystal $CuSO_4$ spin standard. The strong pitch sample contained $4.5 \times 10^5$ spins per gram. The spin concentration determined in this manner is accurate to within ±25% (*6*).

Mössbauer spectra were collected for the EuFe–Y sample after reductions in flowing $H_2$ and CO at 720 K. All spectra were obtained following cooling of the sample to room temperature. The procedures used to collect the Mössbauer spectra were the same as described elsewhere (*1, 3*). In short, an Austin Science Associates spectrometer was employed and the EuFe–Y sample was pretreated and studied in a glass cell with thin Pyrex windows for transmission of $\gamma$ rays. The isomer shift reported here is with respect to metallic iron at room temperature.

## RESULTS

### *EPR Spectroscopy of Na–Y Zeolite*

Three EPR signals may be identified for the Na–Y zeolite sample: (i) a broad asymmetrical signal at $g_{eff} = 2.3$, (ii) a narrow signal at $g_{eff} = 2.1$, and (iii) a sharp signal at $g_{eff} = 4.3$. These signals have been previously identified in commercially synthesized zeolites, and they are due to iron impurities (*7–10*) that originate from the silica used for the zeolite synthesis. They are absent in pure Y zeolite (*9*).

### *EPR Spectroscopy of Eu–Y Zeolite*

*Oxidation.* The $Eu^{3+}$ ions ($4f^6$) have a diamagnetic ground state ($^7F_0$) and conse-

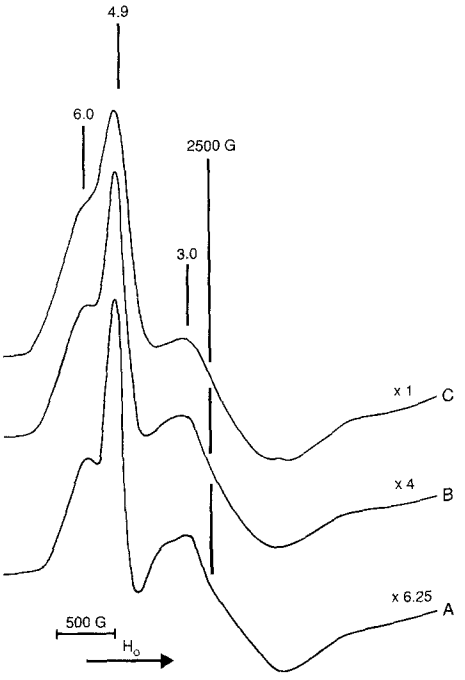


FIG. 1. EPR spectra of $Eu^{2+}$ in Eu–Y reduced with $H_2$ at 773 K (A) for 12 h (300 K), (B) for 120 h (300 K), and (C) for 120 h (77 K).

TABLE 1

Principal EPR Parameters of $Eu^{2+}$ and $Fe^{3+}$ in EuFe–Y Zeolite

| Cation | Temperature (K) | $g_{eff}$[a] | Width (G) |
|---|---|---|---|
| $Eu^{2+}$ | 300 | 6.0 | >250 |
| | | 4.9 | 300 |
| | | 3.0 | Broad |
| | 77 | 6.0 | >250 |
| | | 4.9 | 300 |
| | | 3.0 | Broad |
| $Fe^{3+}$ | 300 | 4.3 | 150 |
| | | 2.3 | Broad |
| | | 2.1 | 250 |
| | 77 | 4.3 | 100 |
| | | 2.2 | Broad |
| | | 2.1 | — |

[a] The error in the reported $g_{eff}$ values is ±0.03.

quently exhibit no ESR spectrum. The ESR signals observed for the oxidized Eu–Y sample are identical to those observed in the Na–Y sample and they are again associated with the $Fe^{3+}$ impurities.

*Reduction.* The spectra obtained after reducing the Eu–Y zeolite at 773 K with either $H_2$ or CO are presented in Figs. 1 and 2. Additionally, the data are tabulated in Table 1. The spectra exhibit a dominant narrow line at $g_{eff} = 4.9$. Other signals, at $g_{eff} = 6.0$ and at $g_{eff} = 3.0$, are also evident. The signal at $g_{eff} = 6.0$ is partially resolved on the low-field side of the principal peak, while the signal at $g_{eff} = 3.0$ is more clearly resolved. Similar results were obtained by Iton *et al.* (*10*) from $Eu^{2+}$ in Y zeolite. Because of the width and overlapping of the peaks the $g$ values are reported to only one decimal place with an error of ±0.03.

The spin concentration of $Eu^{2+}$ in Eu–Y zeolite as a function of extent of reduction was calculated from the X-band EPR spectra. The overall extent of reduction was measured by the weight change using a microbalance (see Table 2). The number of spins per unit cell determined both using EPR and from the average oxidation state

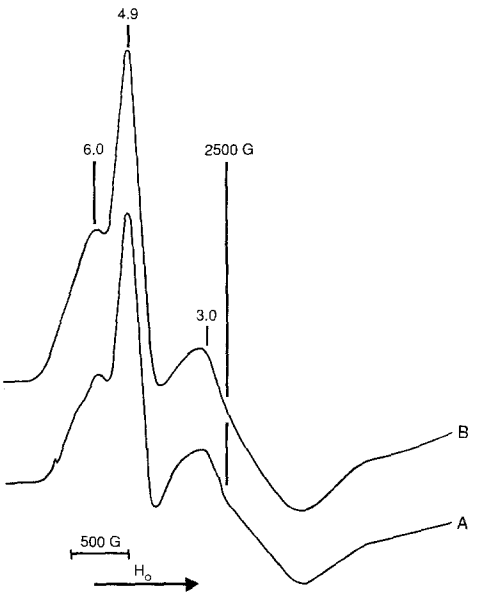


FIG. 2. EPR spectra of $Eu^{2+}$ in Eu–Y reduced at 773 K with (A) $H_2$ for 12 h (300 K) and (B) CO for 4 h (300 K).

TABLE 2

Changes in Principal EPR Spectral Features after Various Treatments for the Europium-Containing Y Zeolites

| Signal[a] | Treatment | | | | |
|---|---|---|---|---|---|
| | Reduction | | | Reaction ($CO/O_2$ = 3) | |
| | (CO) Eu–Y | (CO) EuFe–Y | ($H_2$) EuFe–Y | Eu–Y | EuFe–Y |
| Eu 6.0 | Shoulder | Shoulder | Shoulder | Resolved | — |
| 4.9 | Principal | Principal | Resolved | Resolved | — |
| 3.0 | Resolved | Resolved | Resolved | — | — |
| Fe 4.3 | — | — | — | Resolved | Resolved |
| 2.3 | — | — | — | Resolved | Resolved |
| 2.1 | — | — | — | — | Resolved |

[a] The error in the reported $g_{eff}$ values is ±0.03.

are in agreement when the average oxidation state is 1.4 ± 0.05 (the reader should note that this average oxidation state implies the presence of either $Eu^{1+}$ or $Eu^0$). However, they differ when the average oxidation state of the sample is 2.4 ± 0.05. This may be due to some of the Eu not being detected in the EPR spectra. This phenomenon has been reported for other catalysts (*16*). The principal EPR parameters, effective $g$ values, and width-to-intensity ratio of the peaks for both oxidation states remained unchanged when spectra were collected between 77 and 300 K. The only change in the spectra between these temperatures can be attributed to changes in the equilibrium spin populations, i.e., the absolute peak intensity.

The similarity between samples reduced in either $H_2$ (12 h) or CO (4 h) is shown in Fig. 2. With the exception of a small intensity difference (which is accounted for by the difference in reduction times), the spectra are identical.

*Reoxidation.* Following reduction in $H_2$ for 100 h, Eu–Y zeolite was oxidized at 773 K using 25% $O_2$ in He. Figure 3 shows the spectra of Eu–Y reduced, partially reoxidized (after exposure to flowing $O_2$ for 1 h), and completely reoxidized (80 h exposure). Comparison of the spectra shows that the relative intensity of the principal line ($g_{eff}$ = 4.9) diminishes more rapidly than that of the lines at $g_{eff}$ = 6.0 and 3.0 during reoxidation. This indicates that the $Eu^{2+}$ ions which are responsible for the peak at $g_{eff}$ = 4.9 exhibit different chemistry than those with $g_{eff}$ = 3.0 and 6.0. No trace of $Eu^{2+}$ remained after oxidation for 80 h.

*CO oxidation reaction conditions.* Three types of experiments were carried out to characterize the behavior of Eu–Y zeolite under CO oxidation conditions:

1. Oxidized Eu–Y was allowed to reach stable reaction conditions at 773 K in a flowing gas mixture ($CO/O_2$ = 1 diluted in 75% in He) (oxidizing regime).

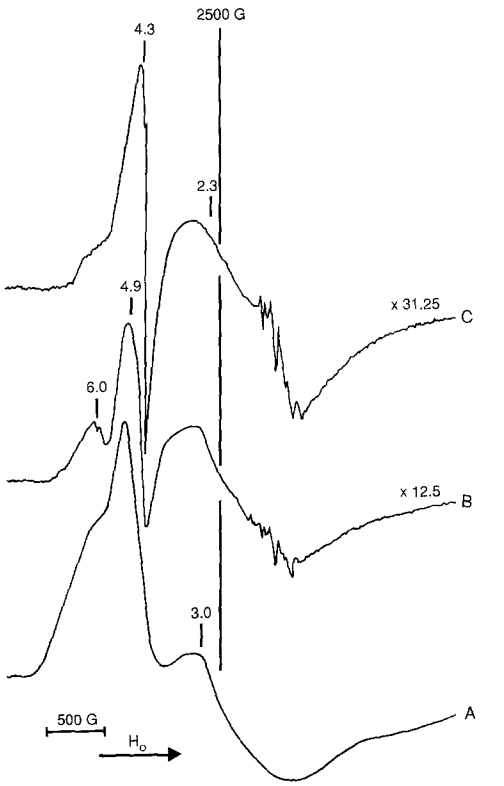


FIG. 3. Effect of the progressive reoxidation of $Eu^{2+}$ in the spectra of Eu–Y (A) after reduction in CO for 120 h at 773 K (77 K), (B) after reoxidation in $O_2$ for 1 h at 773 K (77 K), and (C) after reoxidation in $O_2$ for 80 h at 773 K (77 K).

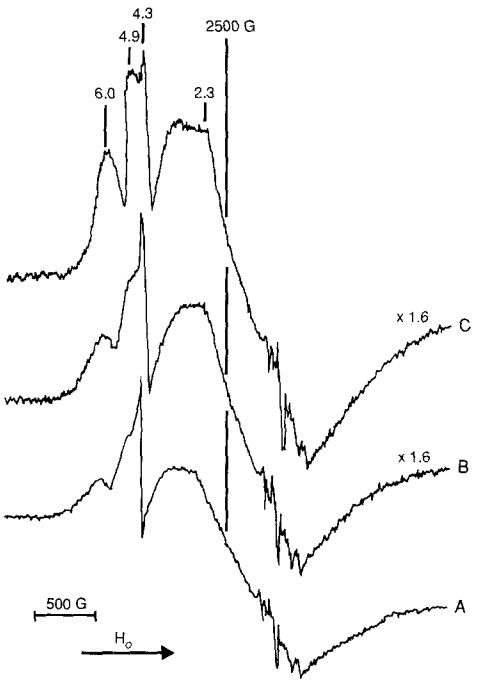


FIG. 4. Behavior of the Eu ions in Eu–Y under reaction conditions according to the EPR spectra: (A) Oxidized Eu–Y was in contact with flowing reactant gases, $CO/O_2 = 1$, for 1 h at 773 K (77 K); (B) the same as (A), but the ratio was $CO/O_2 = 3$ (77 K); (C) reduced sample was exposed to flowing $CO/O_2 = 3$ for 30 min.

2. Oxidized Eu–Y was in contact for 1 h with CO and $O_2$ ($Co/O_2 = 3$ diluted in 75% in He at 773 K) (reducing regime).

3. The sample of experiment 2 was maintained for an additional 40 min under the reaction conditions.

The results of these experiments are given in Fig. 4, and these spectra show that the states of the sample are similar after each of the preceding treatments. That is, the spectra all exhibit resonances at $g_{eff} = 4.9$ and 6.0 ($Eu^{2+}$) along with resonances at $g_{eff} = 4.3$ and 2.3 ($Fe^{3+}$). However, a difference in the $Eu^{2+}$ signal intensity is evident between the spectrum of reduced Eu–Y (Fig. 3A) and the spectra in Fig. 4, the latter being two orders of magnitude lower in intensity. This suggests that a small amount of $Eu^{2+}$ was present during CO oxidation reaction conditions.

*Simulation of EPR Spectra*

Results from computer simulations show an adequate fit of the EPR spectra can be obtained using three anisotropic sites, each with nonaxial symmetry. The best fit to experimental spectra is shown in Fig. 5 and the actual $g$ values, Lorenzian linewidths, and relative concentrations used to calculate the simulated spectrum are given in Table 3. These values were determined to provide the best fit to the experimental spectrum by comparing the simulated first-derivative spectrum with the experimental spectrum. To check the fit the simulated second-derivative spectrum was compared with the experimental second-derivative spectrum. The best fit was determined subjectively through iterative comparisons of the two types of spectra and variation of the input values into the simulation. The second-derivative spectra are not shown as they were used only for fitting purposes.

*Gravimetric Studies of Eu–Y Zeolite*

The criterion for stability of the samples was taken as the reproducibility of the data in oxidation–reduction cycles; i.e., the ox-

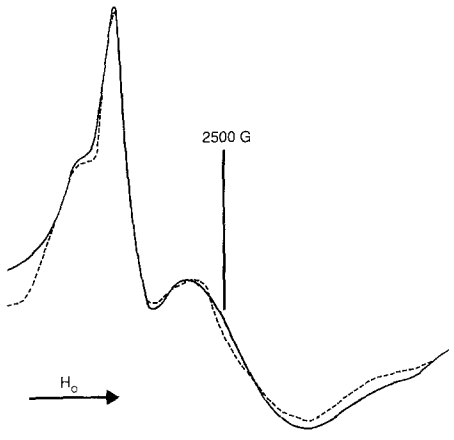


FIG. 5. Comparison of best simulation with experimental spectrum (Fig. 3B).

TABLE 3

Spin Concentration of $Eu^{2+}$ in Eu–Y

| Average Eu oxidation state, microbalance[a] | Spin concentration (spins/unit cell) | |
|---|---|---|
| | Calculated[b] | EPR |
| 1.4 | 5.2 | 6.0 ± 0.75 |
| 2.2 | 10.4 | 3.2 ± 0.40 |
| 2.4 | 7.8 | 3.0 ± 0.35 |
| 3.0 | 0.0 | 0.0 ± 0.25[c] |

[a] The uncertainty in the measurement is ±0.05.

[b] These data were calculated from the microbalance data for average oxidation state. The calculation uses $Eu^{2+}$ as the only Eu species with an EPR resonance, i.e., Eu(III) and Eu(I) having no EPR signal.

[c] Uncertainty here is due to the presence of $Fe^{3+}$.

ygen-carrying capacity should remain constant. Deviation from this criterion can be interpreted as either a collapse of the zeolite structure or a reduction of Eu to the metal and a subsequent migration to the outside of the zeolite. Various oxidation–reduction couples were used at 773 K, i.e., $CO/O_2$, $H_2/O_2$, and $H_2/N_2O$. The results are shown in Fig. 6A. The gas in contact with the zeolite is indicated above the lines corresponding to the steady-state weight, while the time required to reach equilibrium is given below the lines. These data show that Eu–Y was stable, and could be reversibly oxidized and reduced over many cycles. The weight change shows that the amount of oxygen removed or added corresponded to O/Eu = 0.8 ± 0.02 during the reduction in contrast to $Cu^{2+}$–Y zeolite (*17*).

Carbon monoxide oxidation was carried out in the flow microbalance to determine the influence of the overall gas-phase redox potential on the oxidation state of the base-exchange cations. Two reactant gas ratios were used in these experiments, i.e., $r = 1$ and 3, where $r$ is the $CO/O_2$ ratio. The weight of Eu–Y under reaction conditions (see Fig. 6A) was slightly larger than that found for the oxidized state, even when $r = 3$ and the reaction is overall reducing.

The weight change during reduction is shown in Fig. 6B. It is evident that when $H_2$ was used as the reducing gas, a longer time was required to reach equilibrium (100 h)

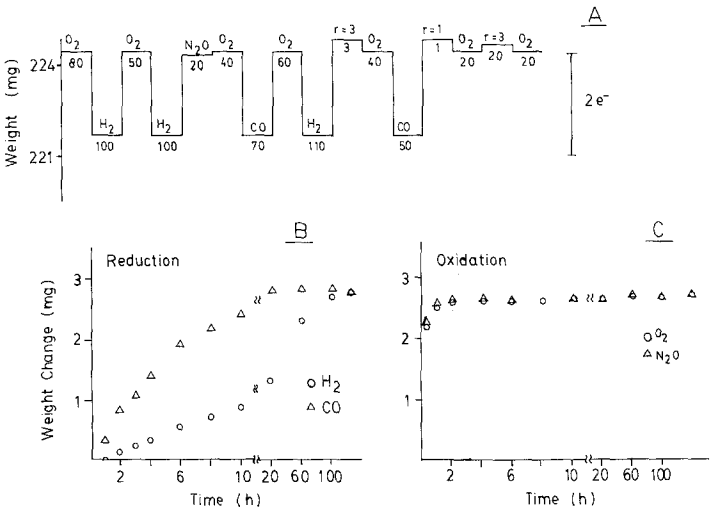


FIG. 6. Flow microbalance studies of Eu–Y zeolite in oxidation–reduction cycles: (A) The lined out weights of Eu–Y under reduction (CO and $H_2$) and oxidation ($N_2O$ and $O_2$); (B) the weight change with time for the reduction in CO (△) and $H_2$ (○): (C) the weight change of the reduced sample with time under oxidation in $O_2$ (△) and $N_2O$ (○).

compared with reduction in CO (40 h). These data are in agreement with the EPR data obtained under identical conditions, i.e., the spectrum of Eu–Y reduced in $H_2$ for 12 h is identical to that obtained after 4 h in CO (Fig. 2).

Oxidation of Eu–Y occurs in two regimes. The first phase is rapid and takes place during the initial 2 h. This accounts for the majority of the total oxygen capacity of the sample. The second part is slow and continues for about 50 h. These data are shown in Fig. 6C. No differences can be found between oxidation using either $O_2$ or $N_2O$, in contrast to results for Fe–Y having a high silicon-to-aluminum ratio (*3*). EPR spectra taken as a function of oxidation time show that the Eu is completely oxidized after about 20 h, while some of the impurity iron is more slowly oxidized.

### *EPR Spectroscopy of EuFe–Y Zeolite*

*Oxidation.* Figure 7 shows the spectra of the oxidized EuFe–Y zeolite. Three signals characteristic of $Fe^{3+}$ in the zeolite structure are evident: (1) a sharp peak at $g_{eff}$ = 4.3, (2) a broad signal at $g_{eff}$ = 2.3, and (3) a narrow signal at $g_{eff}$ = 2.1. A marked temperature effect in the relative intensities and $g$ values of the signals is seen. It must be noted that, in this case, the line at $g_{eff}$ = 2.1 is more intense than in Na–Y.

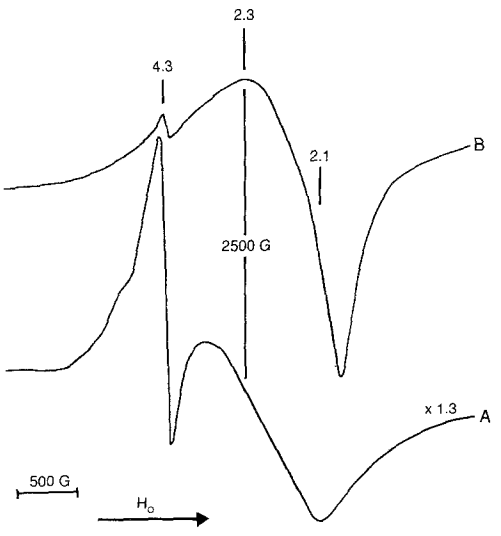


FIG. 7. EPR spectra of $Fe^{3+}$ in oxidized EuFe–Y zeolite (A) at 77 K and (B) at 300 K.

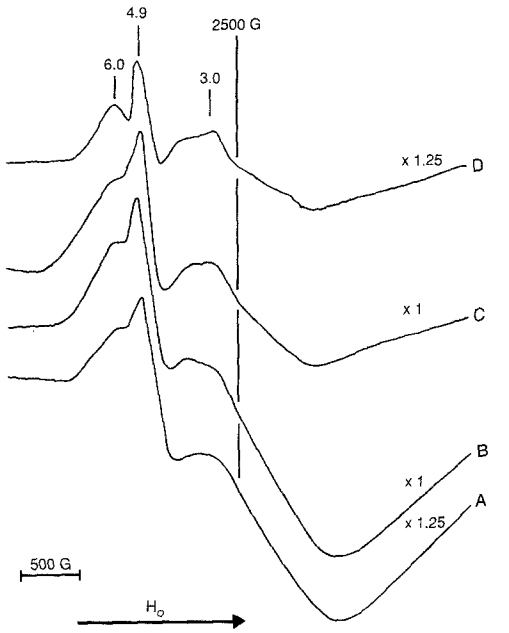


FIG. 8. EPR spectra of $Eu^{2+}$ in EuFe–Y reduced at 773 K with (A) $H_2$ for 1 h (77), (B) $H_2$ for 50 h (77 K), (C) CO for 50 h (77 K), and (D) CO for 1 h (77 K).

*Reduction.* The spectra of EuFe–Y treated for 1 h with either CO or $H_2$ (partially reduced) or 50 h (completely reduced to $Fe^{2+}$ and $Eu^{2+}$) are presented in Fig. 8. In each case, the spectrum consists of $Eu^{2+}$ signals at $g_{eff}$ = 6.0, 4.9, and 3.0. No signal due to $Fe^{3+}$ was observed even when the reduction time was 1 h. It can be seen that the relative signal intensities are different depending on whether $H_2$ or CO was used as the reducing agent, especially after 50 h. In the case of reduction by $H_2$, the principal peak was at $g_{eff}$ = 4.9, as in reduced Eu–Y, while in the case of reduction by CO, the signal at $g_{eff}$ = 3.0 decreased markedly. This difference is notable even when the EuFe–Y was treated with CO for just 1 h.

*CO reaction conditions.* The EPR spectrum of EuFe–Y was collected after the sample reached steady state at 773 K in a

flowing reactant gas mixture with He. The value of $r$ for $CO/O_2$ was 3, which is overall reducing. However, the spectrum after this treatment was comparable with that of an oxidized sample, except that the signal at $g_{eff} = 2.1$ was resolved in the spectrum of the oxidized sample. This behavior is in agreement with previous microbalance studies and infrared spectroscopy of NO adsorption on this catalyst (*11*), which showed that EuFe–Y is essentially in a fully oxidized state under these reaction conditions.

### *Mössbauer Spectroscopy of EuFe–Y Zeolite*

Room-temperature $^{57}Fe$ Mössbauer spectra of EuFe–Y are shown in Fig. 9 after various treatments. The sample was first treated in $O_2$ at 720 K and subsequently reduced in $H_2$ for 5 h at this same temperature. The sample was then cooled in $H_2$ to room temperature, and the spectrum in Fig. 9A was collected. This spectrum is composed of two quadrupole split doublets: a relatively intense component denoted as the "inner doublet" with a small isomer shift and quadrupole splitting, and a weaker component denoted as the "outer doublet"

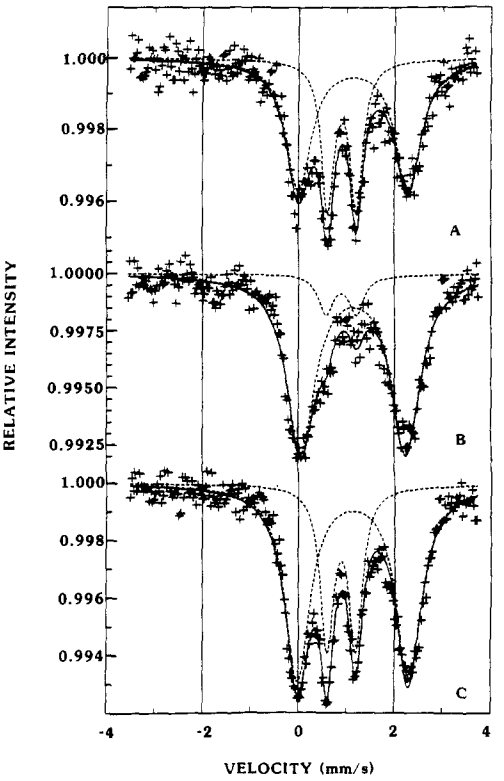


FIG. 9. Room-temperature Mössbauer spectra of $^{57}Fe$ in EuFe–Y zeolite: (A) oxidized sample reduced in $H_2$ for 5 h at 720 K and cooled in $H_2$; (B) sample in (A) was treated with CO for 1 h at 720 K and cooled in CO: (C) sample in (B) was treated in flowing He and the temperature raised to 720 K for 15 min and cooled in He.

TABLE 4

Simulation Parameters for Fig. 5

| Parameter[a] | $g_{eff}$ | | |
|---|---|---|---|
| | 6.0 | 4.9 | 3.0 |
| $g_1$ | 7.452 | 5.08 | 3.065 |
| $g_2$ | 6.61 | 4.36 | 2.455 |
| $g_3$ | 1.455 | 1.385 | 2.069 |
| $w_1$ | 225 | 175 | 1295 |
| $w_2$ | 380 | 295 | 1257 |
| $w_3$ | 250 | 350 | 1550 |
| %[b] | 1.54 | 9.26 | 89.20 |

[a] $g_1$, $g_2$, and $g_3$: $g$ values of the nonaxially symmetric site. $w_1$, $w_2$, and $w_3$: Lorenzian linewidths, in gauss, for the corresponding $g$ values listed above.

[b] Percentage contribution of each site to the total spectrum.

having a larger isomer shift and quadrupolar splitting. This is in agreement with our previous results (*1*) and indicates that europium forces most of the iron from site I (where it is normally present in Fe–Y) to sites I′, II′, II, and/or III′.

The above EuFe–Y sample was then treated for 1 h with CO at 720 K and cooled to room temperature in CO, and the Mössbauer spectrum shown in Fig. 9B was collected. It is apparent that the intensity of the outer doublet has increased at the expense of the inner doublet compared with the spectrum in 9A. This change may be interpreted in terms of a larger fraction of the ferrous cations being in site I after CO

treatment. However, CO adsorbed on ferrous cations at site II can also produce a Mössbauer spectroscopy component similar to the outer doublet (*1, 3*).

To distinguish between these two possible explanations for the growth of the outer doublet, the sample was subsequently treated in flowing He for 15 min at 720 K and cooled to room temperature, and the spectrum shown in Fig. 9C was recorded. It is clearly seen that the intensity of the outer doublet has decreased, compared with spectrum 9B. However, the intensity of the outer doublet in spectrum 9C is higher than that in spectrum 9A. More quantatively, the outer doublet accounts for 64, 89, and 70% of the total spectral area in Figs. 9A, B, and C, respectively.

It is possible that the sample of spectrum 9C still contains CO adsorbed on ferrous cations, thereby accounting for the higher intensity of the outer doublet compared with spectrum 9A. However, the results may also be explained by the possibility that a larger fraction of the ferrous cations is located at site I after CO reduction compared with the case after $H_2$ reduction. These possibilities are discussed next.

## DISCUSSION

### *Eu-Exchanged Y Zeolite*

Based on previous studies (*9, 11*), the $Eu^{3+}$ cations present after initial oxidation of Eu–Y at 773 K are expected to be found in the sodalite cages at site I′. These cations retain an extra framework OH ligand in addition to interacting with the framework oxygen, as found for $Gd^{3+}$ (*9*). The presence of the OH group is supported by the infrared work of Rabo *et al.* (*12*) who found that OH remained bonded to $Ce^{3+}$ even after vacuum calcination at 1173 K. This apparently did not occur with divalent cations, i.e., $Ca^{2+}$. Moreover, Olson *et al.* (*13*) have found that trivalent cations were preferably located at site I′ rather than site I.

Reduction of $Eu^{3+}$ in Y zeolite has been previously shown to be difficult. Mössbauer spectroscopy studies indicated that at 725 K no reduction occurs over several hours (*1*), while at 773 to 823 K the $Eu^{3+}$ is reduced to $Eu^{2+}$ (*15*). More recent microbalance studies indicate that at 773 K $Eu^{3+}$ may be reduced to an undetermined oxidation state below 2+ (*11*). However, this extent of reduction required extended periods (80 h) as well as higher temperature. It is also possible that the apparent reduction below the divalent state may be due to the removal of OH groups associated with the $Eu^{3+}$ upon reduction.

The EPR spectra of reduced Eu–Y contain three distinct resonances at $g_{eff}$ of 6.0, 4.9, and 3.0, showing no change in relative intensity between 4 and 120 h of $H_2$ reduction. Iton *et al.* (*10*) has previously shown that the first two resonances are associated with a distribution of $Eu^{2+}$ cations at sites I′, II′, and II, while the third is associated with $Eu^{2+}$ at site I. Additionally, the relative intensity of the resonances does not change upon slow cooling to 77 K or slow warming from 77 to 300 K, indicating that the cations are immobile over this temperature range.

The reoxidation experiments in Fig. 3 show that the $Eu^{2+}$ ions responsible for the signal at $g_{eff} = 4.9$ are more easily oxidized than the others. This indicates that the $Eu^{2+}$ responsible for this resonance is at a site which both is readily accessible to the oxidant and has a sufficiently open coordination environment for oxidation to occur readily. The most accessible of the sites Iton *et al.* (*10*) have associated with this signal is site II, in the supercage. This site, like site II′, is coordinated to the lattice on one side and has the possibility of a more open coordination environment on the other side. Unlike site II′, which has the possibility of an interaction with a cation at site I′ through a bridging oxygen ion, site II is the more likely site to be associated with the $g_{eff} = 4.9$ resonance.

Under CO reaction conditions, the spectra of Eu–Y are similar, irrespective of whether the sample is in a fully oxidized or

reduced state at the beginning of the reaction and independent of the ratio $CO/O_2$ (see Fig. 4). Furthermore, the low intensity of the EPR signal indicates that the sample is operating in a nearly fully oxidized state. It is clear from these data that the $Eu^{2+}$ ions responsible for the EPR signals with $g_{eff}$ equal to 4.9 and 6.0 are present. The signal with $g_{eff}$ equal to 3.0 is not seen, irrespective of whether the starting material is fully oxidized or reduced, or whether the gas-phase environment is overall oxidizing ($CO/O_2 = 1$) or reducing ($CO/O_2 = 3$). This is convincing evidence that the cations at site I are readily oxidized, but are difficult to reduce. The cations exhibiting signals at higher $g$ values must be capable of undergoing reduction more easily as they are present even under reaction conditions which are overall oxidizing. Microbalance studies indicate that the catalyst is essentially fully oxidized (Fig. 6B) under all reaction conditions, consistent with the low intensity of the EPR spectra. Furthermore, the presence of a small number of $Eu^{2+}$ cations can be reconciled with the gravimetric results by infrared studies (*11*) which show that adsorbed CO and $CO_2$ are present on the catalyst (these species increase the weight of the sample).

The relative populations of the sites in the reduced state were determined by simulating the X-band spectra. The simulation (Fig. 5 and Table 3) shows that 89% of observed $Eu^{2+}$ is located in site I. Thus, only 11% of the Eu observed is in sites which are potentially catalytically active. Indeed, the activity of Eu–Y for CO oxidation or $N_2O$ decomposition has been shown to be among the poorest of a wide variety of catalysts studied (*1*).

Comparison of total spin concentrations with average oxidation states from microbalance data shows some inconsistencies. When the microbalance data show the average oxidation state is below 2+, the calculated number of free electrons is in agreement with the ESR spin concentration. However, when the microbalance data show an average oxidation state between 2.2 and 2.5, there is a two- to threefold excess in the number of calculated free electrons compared to the number observed by ESR. This can be rationalized by remembering that in ESR the local magnetic environment of the free electron can be strongly influenced by its surroundings, particularly if those surroundings contain any form of magnetism other than diamagnetism. In Fe–Y zeolite, a redox site has been identified as two cations in sites I′ and II′. The redox cycle involves the addition and removal of a bridging oxygen between the two cations. If we assume that this is also true in Eu–Y (and ESR shows these sites are occupied by $Eu^{2+}$) then the two Eu cations are about 0.4 nm apart. These sites are sufficiently close to undergo both electron–electron exchange and very strong dipolar broadening. The combined effects of both interactions, but particularly the exchange interaction, leads to a deviation from the expected spin concentration. This has been observed for supported Mo catalysts (*16*).

The reduction rate of Eu–Y depends strongly on the reducing gas. Reduction carried out with CO is faster than when $H_2$ is used (see Fig. 4). Kasai and Bishop (*14*) have reported that europium-exchanged zeolites catalyze the thermochemical decomposition of water. They postulate a mechanism that involves europium undergoing oxidation during $H_2O$ decomposition, but which can then be reduced by the product $H_2$, resulting in an alternation between 2+ and 3+ oxidation states. Since water is a product of catalyst reduction by $H_2$, the above reaction would result in the reduction process being inhibited by the product with $H_2$ as a reductant, but not with CO.

*EuFe–Y Zeolite*

When Fe is coexchanged into Y zeolite, the two cations compete for the exchange sites. Previous infrared studies (*11*) of reduced EuFe–Y exposed to NO show that the location of the $Fe^{2+}$ cations depends on the reducing gas used. The EuFe–Y sample

reduced with $H_2$ shows nitric oxide stretching IR bands due to ferrous cations at sites II, II′, and III′ upon initial exposure to NO: however, when the sample is reduced with CO, the only IR bands observed upon initial exposure to NO are due to ferrous cations at sites II and II′. (Upon prolonged exposure to NO at room temperature, ferrous cations migrate from site I to site III′ for the sample subjected to either reduction step.) From these results it was suggested that more europium cations were present at site I for the sample reduced in $H_2$, thereby forcing a larger fraction of the ferrous cations to site III′. Indeed, the EPR spectra of the $H_2$-reduced EuFe–Y sample show a higher initial intensity for the signal with a $g$ value equal to 3.0, and this signal corresponds to $Eu^{2+}$ cations at site I. Furthermore, the above conclusion is consistent with the Mössbauer spectroscopy results of the present study. Specifically, the EuFe–Y sample reduced with $H_2$ shows a weaker outer doublet signal than the sample reduced with CO, and the outer doublet is due to ferrous cations at site I.

It is observed in this study that the EPR signal with $g$ value equal to 2.1 for oxidized EuFe–Y sample is more intense than that observed for Na–Y and Eu–Y. One can thus conclude that this signal is associated with the exchanged Fe, as opposed to iron impurities from the synthesis. Unfortunately, this is the only signal observed for $Fe^{3+}$ and upon reduction it disappears; therefore, this signal provides little new information regarding the distribution of the iron among the sites it may occupy.

## CONCLUSIONS

The experimental results and arguments put forward in this paper indicate that $Eu^{2+}$ in Eu–Y and EuFe–Y zeolites is located at sites I, I′, II, and II′, but that it prefers site I. This Eu siting forces the Fe to sites of lower coordination in the sodalite unit and the supercage, as was demonstrated in previous Mössbauer spectroscopy and infrared studies (*1, 11*). Finally the cation sitings can be altered by changing the reducing gas from $H_2$ to CO.

## ACKNOWLEDGMENTS

The authors express their gratitude to the National Science Foundation for Grants CBT-8414662 and CBT-8810149 which supported this work and to the Union Oil Foundation which provided partial support for one of us (M.A.U.).

## REFERENCES

1. Aparicio, L. M., Ulla, M. A., Millman, W. S., and Dumesic, J. A., *J. Catal.* **110,** 330 (1988).
2. Petunchi, J. O., and Hall, W. K., *J. Catal.* **78,** 327 (1982).
3. Aparicio, L. M., Fang, S. M., Long, M. A., Ulla, M. A., Hall, W. K., Millman, W. S., and Dumesic, J. A., *J. Catal.* **104,** 381 (1987).
4. Aparicio, L. M., Fang, S. M., Long, M. A., Ulla, M. A., Hall, W. K., Millman, W. S., and Dumesic, J. A., *J. Catal.* **108,** 233 (1987).
5. Nilges, M., Ph.D. thesis, University of Illinois, 1979.
6. Asycough, P. B., "Electron Spin Resonance in Chemistry." Methuen & Co. Ltd., London, 1967.
7. Derouane, E. G., Mestdagh, M., and Vielvoye, L., *J. Catal.* **33,** 169 (1974).
8. McNicol, B. D., and Pott, G. T., *J. Catal.* **25,** 223 (1972).
9. Trif, E., Petrisor, S., Strugaru, D., Vass, D., and Nicula, A., *in* "Proceedings, Congr. Ampere 17th, 1973," p. 214.
10. Iton, L. E., and Turkevich, J., *J. Phys. Chem.* **81,** 435 (1977).
11. Ulla, M. A., Aparicio, L. M., Dumesic, J. A., and Millman, W. S., *J. Catal.* **117,** 237 (1989).
12. Rabo, J. A., Angell, C. L., Kasai, P. H., and Schomaker, V., *Discuss. Faraday Soc.* **41,** 328 (1966).
13. Olson, D. H., Kokotailo, G. T., and Charnell, J. F., *J. Colloid Interface Sci.* **28,** 305 (1968).
14. Kasai, P. H., and Bishop, R. J., Jr., U.S. Patent No. 3,963,830.
15. Samuel, E. A., and Delgass, W. N., *J. Chem. Phys.* **62,** 1590 (1975).
16. Abdo, S. A., and Hall, W. K., *J. Phys. Chem.* **80,** 2431 (1976).
17. Petunchi, J. O., and Hall, W. K., *J. Catal.* **80,** 403 (1982).